ANDOYA CAMPAIGN – DATA ACQUISITION REPORT

Prepared by	Laura Warwick
Document Type	TN - Technical Note
Reference	
Issue/Revision	1 . 0
Date of Issue	02/06/2022
Status	N/A

→ THE EUROPEAN SPACE AGENCY

APPROVAL

Title	Andoya Campaign – Data Acquisition Report		
Issue Number	1	Revision Number	0
Author	Laura Warwick	Date	02/06/2022
Approved By		Date of Approval	

CHANGE LOG

Reason for change	Issue Nr	Revision Number	Date

CHANGE RECORD

Issue Number	1	Revision Number		0
Reason for change		Date	Pages	Paragraph(s)

DISTRIBUTION

Name/Organisational Unit

Table of Contents

→ THE EUROPEAN SPACE AGENCY

1. INTRODUCTION

This document reports on the deployment of the new FINESSE instrument to the ALOMAR Observatory in Nordland, Norway. The report begins with an overview of the campaign and the aims of the campaign. Section 2 describes the measurements undertaken including a description of the FINESSE instrument, the other instrumentation, and a chronology of the measurements. Section 3 describes each of the six measurement days in detail including the conditions and the measurements taken. Sections 4 and 5 describe the method of spectral calibration and show some example calibrated spectra. An assessment of the instrument performance is conducted in section 6. Section 7 contains conclusions and suggestions for the use of the data and finally section 8 contains an explanation of the format of the data provided from the campaign.

1.1. Overview of the campaign

In late 2022 Imperial College London were approached by ESA with the opportunity to deploy the Far-infrared Spectrometer for Surface Emissivity (FINESSE) in support of the development of the Universal Radiation Spectrometer (UNIRAS) and the FORUM mission. The deployment of FINESSE was able to piggy-back on the existing MC2-ICEPACKS campaign organised by the University of Oslo. The aim of the MC2-ICEPACKS campaign was to investigate the distribution of Arctic cloud phase and use this gained knowledge to further constrain Earth System Models. The MC2-ICEPACKS campaign consisted of a ground-based segment and airborne measurements facilitated by the INCAS Atmoslab aircraft.

The campaign took place between Monday 6th February and Friday 17th March 2023 and was based at the ALOMAR Observatory, Andøya Space, Andenes, Norway.

1.2. Aim of the campaign and deliverables

The aim of the FINESSE deployment was to support the development of the UNIRAS spectrometer by testing several aspects of the design in the field and to support the FORUM mission through the acquisition of novel datasets including far-infrared radiance

measurements, in-situ measurements of ice cloud properties and additional atmospheric measurements.

Therefore, the objectives of the campaign were to

1. Deploy the new FINESSE spectrometer to an Arctic environment;
2. Investigate the stability of FINESSE and the performance of the calibration system in harsher operating conditions;
3. Measure the downwelling radiative signatures of ice clouds co-incident with in-situ measurements;
4. Measure the radiance emitted by snow and ice surfaces for the retrieval of far-infrared surface emissivity;
5. Measure the downwelling radiance of other scenes.

The deliverable from the campaign as specified by the contract change notice was a calibrated radiance dataset suitable for inversion for the retrieval of atmospheric or surface properties.

2. MEASUREMENTS UNDERTAKEN

2.1. Instrumentation

2.1.1. FINESSE

FINESSE is a new infrared spectrometer developed by Imperial College London with funding from the UK National Centre for Earth Observation. FINESSE is designed to make in-situ measurements of far-infrared surface emissivity however the flexibility of the FINESSE pointing and calibration system means that the instrument can also be used to measure far-infrared radiation in an uninterrupted range of angles from nadir to zenith.

FINESSE consists of a Bruker EM 27 Fourier transform infrared spectrometer coupled with a calibration and pointing system designed and built at Imperial College London. The design of this calibration and pointing system will be adapted for the UNIRAS instrument. FINESSE has a spectral range of 400 to 1600 cm^{-1} (6.3 to 25 μm) and a maximum nominal resolution of 0.5 cm^{-1}. This is achieved by using a diamond input window, potassium bromide beam splitter

and extended MCT detectors. Extended MCT detectors will also be used for UNIRAS. FINESSE has a field of view of 38 mm at the input window and a beam divergence of 1.7°. The acquisition time for each spectrum is around 1.5 s.

The calibration and pointing system consists of a heated black body cavity (HBB), a cold black body cavity (CBB), which is at ambient temperature, and a gold pointing mirror controlled by a stepper motor. The HBB and CBB are cylindrical cavities constructed from copper. The internal walls of the cavities are coated with Aeroglaze Z306 paint and Vantablack disks are installed at the back faces of the cavities. The temperatures of the black body cavities are monitored using two platinum resistance thermometers (PRTs). One PRT is embedded in the back face of each cavity and one PRT is located in the side wall of each cavity, close to the opening.

The spectrometer and calibration system are housed in an aluminium box on which are mounted a Vaisala PTU300 pressure, temperature, humidity sensor and a Vaisala GMP343 CO_2 sensor. For deployment in arctic conditions an additional heater and additional insulation were added to the aluminium box. FINESSE is currently powered via 230 V mains power and the associated electronics used to power and control FINESSE are housed in an electronics box which is also insulated and heated to withstand arctic temperatures. A custom graphical user interface is used to control FINESSE. This interface allows the user to automate the pointing and data acquisition. Figure 1 shows several views of the FINESSE instrument in the laboratory.
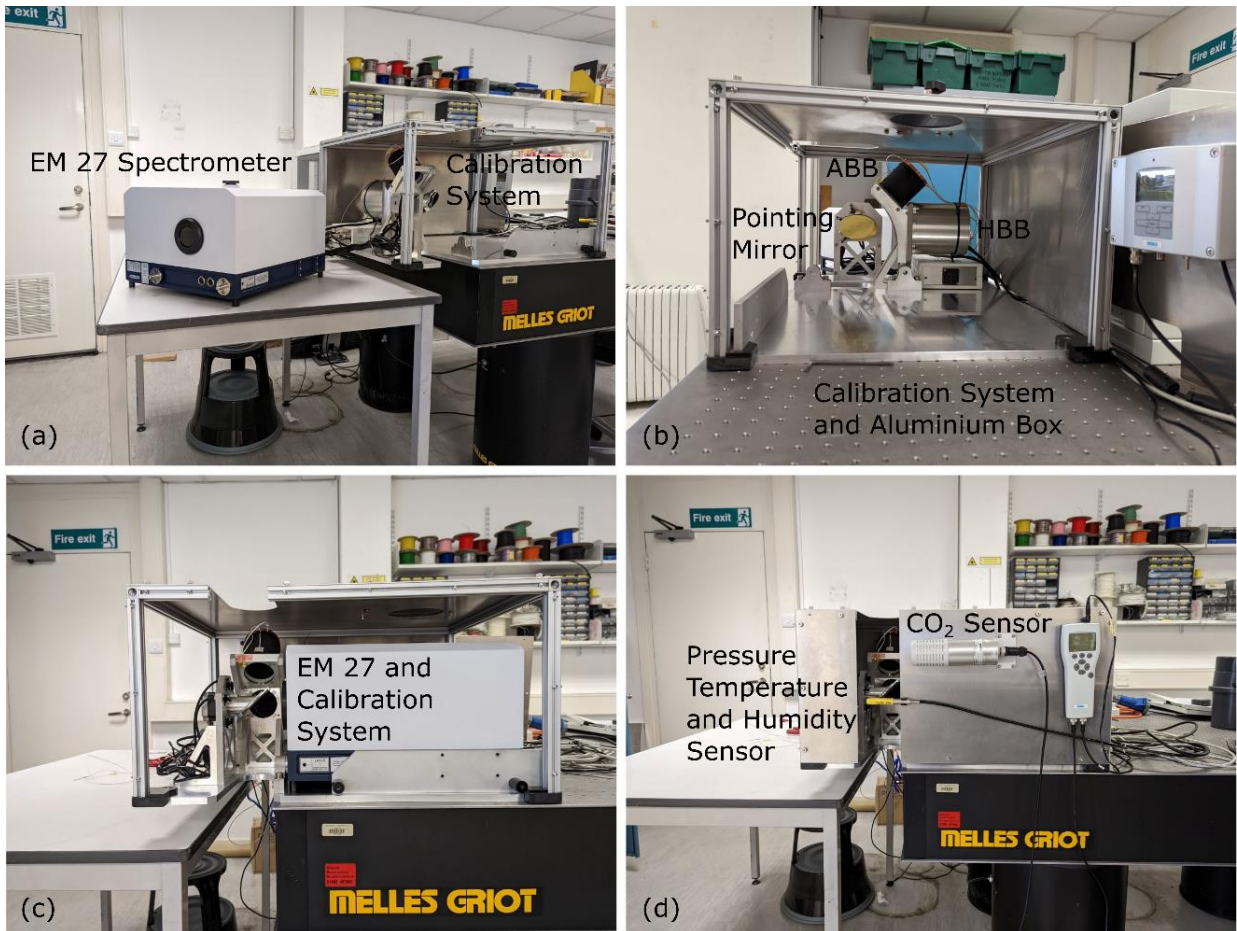
Figure 1. Labelled photos of FINESSE. (a) shows the EM 27 spectrometer outside the calibration system, (b) shows a second view of the calibration system, (c) shows the EM 27 and calibration system together and (d) shows the aluminium box that houses FINESSE and the additional environmental monitoring. From Warwick (2023).

In usual operation FINESSE will view the target scene interspersed with frequent views of its calibration cavities. In the set up used on this campaign, FINESSE recorded 40 individual interferograms for each view position in was programmed to view. This meant each view position lasted for roughly one minute. The order of the view positions was generally

1. Hot black body
2. Cold black body
3. Scene (1)
4. Scene (2)
5. Hot black body
6. Cold black body
7. Etc…

THE EUROPEAN SPACE AGENCY

The number of scene views between the calibration views changed depending on the purpose of the measurements.

FINESSE was installed at the ALOMAR Observatory on Ramnan Hill. The location of the observatory is 69°16' N, 16° 0' E and the observatory is 372 m above sea level. Figure 2 shows the location of the observatory. FINEESE was housed in a garage on the north side of the observatory. From this garage FINESSE could be wheeled outside to make observations. Figure 3 was taken on the 17th of March and shows this setup. The surface in front of the garage slopes away from the building and a ramp was used with jacks to level the instrument, using a spirit level.
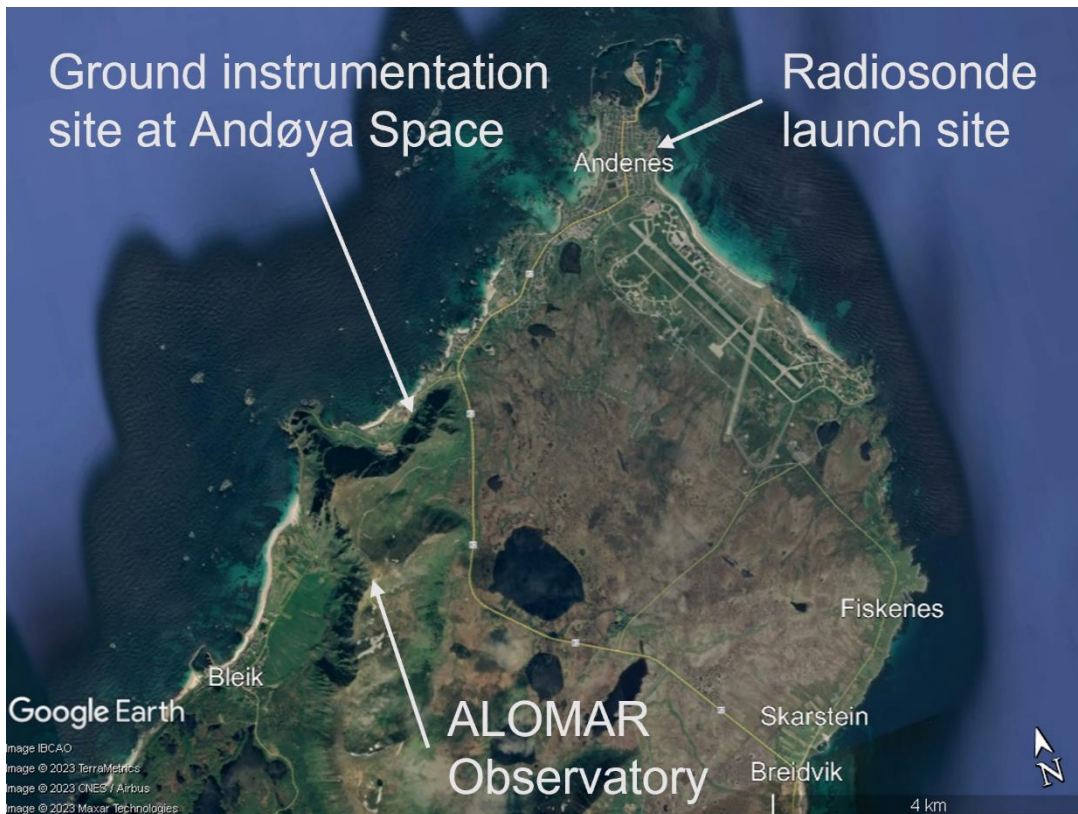

Figure 2. Satellite view of the measurement site showing ALOMAR observatory, the ground instrumentation site at Andøya space and the radiosonde launch site.

Figure 3. FINESSE set up for measurements outside ALOMAR observatory. Photograph taken at 08:44UTC on 17th of February 2023 by Jon Murray.

2.1.2. Other Instrumentation

As part of the MC2-ICEPACKS campaign both ground-based and airborne measurements were undertaken throughout the campaign.

2.1.2.1. Airborne

Airborne measurements were carried out by the INCAS Atmoslab aircraft. The aircraft was carrying a Hawkeye Combination Cloud Particle Probe (SPEC, 2012) and a Cloud, Aerosol and Precipitation Spectrometer (CAPS) system (Calcan et al., 2020). Measurements are also made of outside air temperature, aircraft position and aircraft altitude. These data will be processed by the University of Oslo to provide ice water content, extinction, and crystal habits.

2.1.2.2. Ground Based

Ground based measurements were made using the ALOMAR tropospheric LiDAR installed at the ALOMAR observatory (Schäfer et al., 2022). These observations were made as part of the MC2-ICEPCAKS campaign and the data will be processed by the University of Oslo.

→ THE EUROPEAN SPACE AGENCY

Further ground-based instruments were installed at a ground instrumentation site at Andøya space centre, see figure 2. These include a HATPRO temperature and humidity profiler (RPG-Radiometer Physics, 2013) and a ceilometer with depolarisation (Vaisala, 2022).

Radiosondes were released from a metrological site neat Andenes airport (see figure 2). There were two routine releases each day with further releases scheduled during periods where measurements were taking place.

2.2. Chronology of measurements taken

To fulfil the campaign objectives measurements were taken during periods of clear sky and when there was cirrus overhead without underlying low or mid-level clouds. This limited the possible measurement time to six days during the campaign. Measurements were ended on the 8th of March by a power supply failure within the EM 27 however this did not significantly reduce the quantity of data collected. Table 1 summarises the measurements taken over the course of the campaign. Overall including the calibration views, the data consists of 11.5 hours measuring downwelling spectra in the presence of cirrus clouds, 1.5 hours of measuring downwelling spectra in clear sky conditions and 14 hours measuring spectra for emissivity retrieval.

Date	Conditions	Measurements Taken	Duration of observations
17 Feb	Patchy cirrus clouds	Zenith	5h30
20 Feb	Low clouds and clear sky	Zenith	2h
21 Feb	Snow emissivity	Emissivity	5h30
22 Feb	Frontal cirrus clouds	Zenith	3h
7 March	Snow emissivity and cirrus clouds	Emissivity and Zenith	5h30
8 March	Snow and ice emissivity and clear sky	Emissivity and Zenith	8h

Table 1. Summary of radiance data acquired during the campaign.

3. DATA AQUIRED BY TYPE

THE EUROPEAN SPACE AGENCY

The radiance data taken during the campaign can be split into two types of measurements, zenith measurements and emissivity measurements. The zenith measurements consist of measurements of the downwelling radiance in a variety of conditions including cirrus, clear sky and low clouds. The emissivity measurements consist of upwelling radiance measurements from several snow and ice surfaces at angles of 35° and 50° and downwelling radiance measurements at angles of 145° and 130°. The emissivity measurements took place under clear sky conditions.

3.1. Zenith

3.1.1. 17th February 2023 0730 – 1250 UTC Cirrus 1

Thin cirrus was forecast above ALOMAR observatory with no low or medium cloud. FINESSE undertook zenith view measurements over the period 0730 to 1250 UTC. The INCAS aircraft overflew the observatory to sample the cirrus between 0800 and 0845 UTC.
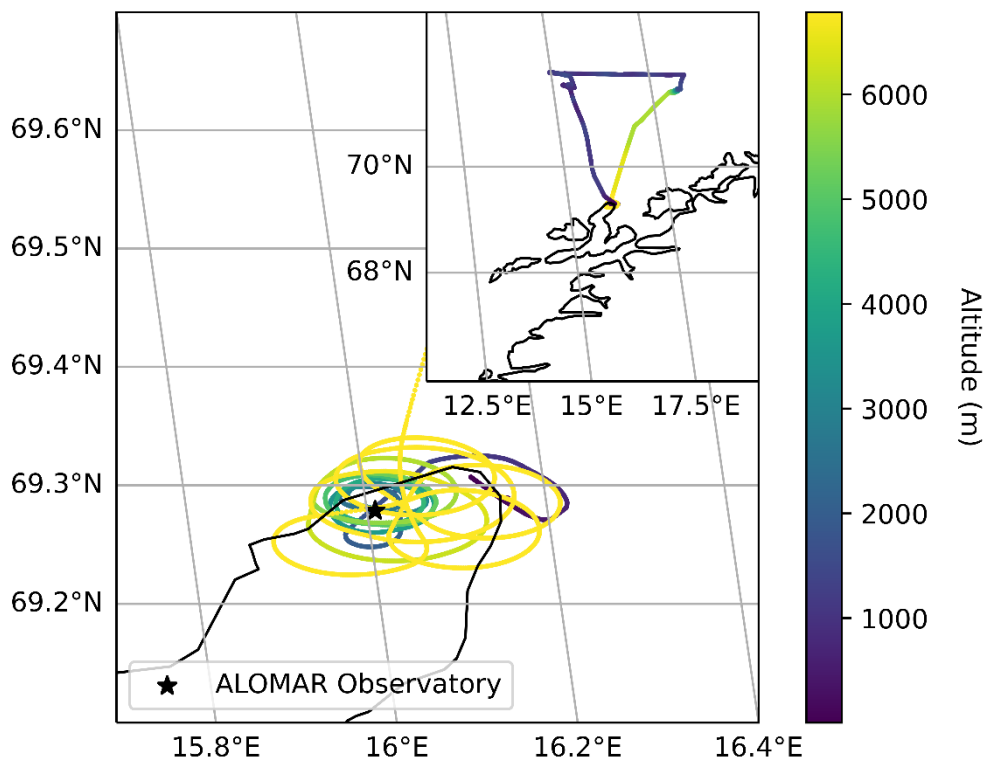

Figure 4. The trajectory of the INCAS aircraft over the ALOMAR observatory on 17th Feb 2023. The colour represents the altitude of the aircraft. The inset plot shows the trajectory of the whole science flight.

Figure 4 shows the trajectory of the aircraft over the observatory. Figure 5 shows pictures captured from the observatory of the sky above FINESSE during and after the overpass. As

can be seen from the photos this cirrus was thin and patchy, so the aircraft performed several loops over the observatory at a hight of roughly 6700 m to try to sample the cirrus. The aircraft then departed to the north to fulfil other campaign objectives.

As aircraft are not allowed to fly over the ALOMAR observatory when the LiDAR are operating, the tropospheric LiDAR was only operational after 0912 UTC. There was a radiosonde launch from Andoya airport at 0808 UTC. The data from this (and all radiosondes) are made publicly available by the Norwegian Metrological Institute (https://thredds.met.no/thredds/catalog.html). Ground based measurements from the HATPRO installed at the ground instrumentation site were ongoing throughout the day. The ceilometer with depolarisation installed at the ground instrumentation site was not working however ceilometer data without depolarisation are available from the ceilometer at Andøya airport. This is also made available by the Norwegian Metrological Institute. Further in-situ data is available from the ALOMAR weather station.
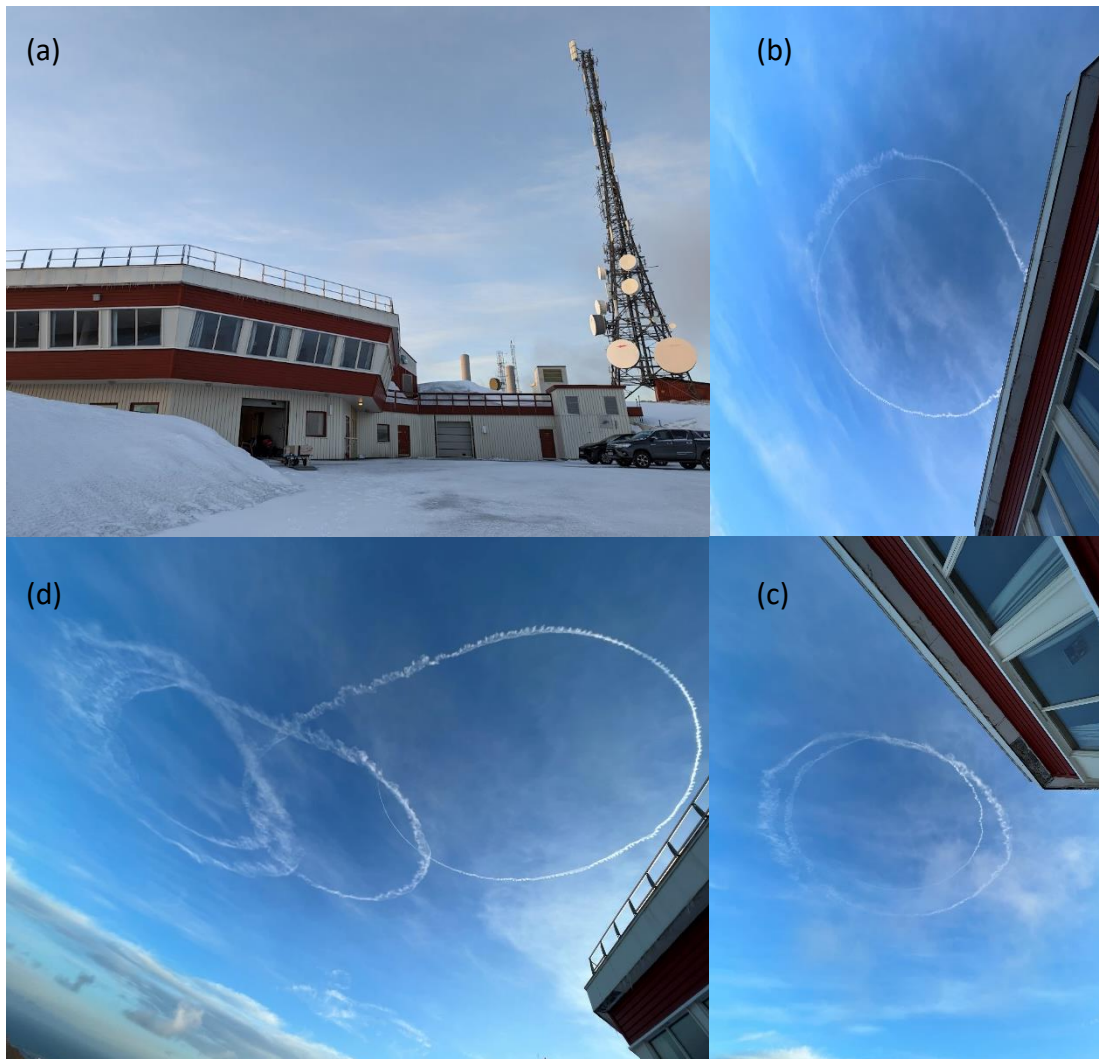
Figure 5. Photos of the sky above the observatory during and after the INCAS aircraft overpass. (a) FINESSE set up to take measurements 0745 UTC, photograph Laura Warwick (b,c,d) the sky above the observatory during the INCAS overpass at 0824, 0827 and 0837 UTC respectively, photographs Jon Murray.

From both the plane and the ground it was clear that the cirrus was very thin and changing rapidly. This will be a very complex case study but may prove to be a good contrast against the second cirrus flight on the 22nd February, outlined in section 3.1.3.

3.1.2. 20th February 2023 1130 – 1330 UTC Low intermittent clouds 1

Before the measurements, heaters were added to FINESSE to maintain critical electronic components above 0C as the temperatures at ALOMAR were forecast to drop to lows of -7°C. The 24 V power supply for the stepper motor was used to provide power for 2x15 W heater pads. One 15 W heater was added to the side of the black electronics box to support the self-

heating from the rack mounted power supplies. Subsequent measurements confirmed that the 15W heater was sufficient to maintain the temperature of the electronics box above 0°C, even when the external temperature dropped to -12°C on subsequent days. The second 15 W heater was placed on the aluminium baseplate below the stepper motor controller housing, to add additional heating to this component. This is likely not ideal as most of the heating is conducted away from the location through the baseplate, however additional foam insulation on the controller housing was also added and residual heating from the outflow of the hot blackbody aperture was also diverted towards the stepper motor controller housing. The combination of these changes was sufficient to maintain the air temperature near the controller near 0°C during subsequent measurements, dropping no lower than -2°C when the ambient temperature was -12°C. No adverse operational behaviour was observed for the controller at these low temperatures.

The weather forecast had suggested that there would be clear skies over ALOMAR however on the day of the measurements there were low and medium clouds making emissivity measurements impossible. FINESSE therefore made zenith measurements between 1130 and 1330 UTC as various clouds went over the observatory. Figure 6 shows the sky over the observatory. This data may be of interest for intercomparison with the HATPRO measurements at the ground instrumentation site. The HATPRO includes a Heitronics infrared radiometer. The measurements from this radiometer can be compared to those from FINEESE by applying the Heitronics spectral response function to the calibrated FINESE data.

Figure 6. The sky above ALOMAR on the 20th February, left at 11:05 UTC and to the right at 12:46 UTC. Photographs Jon Murray.

3.1.3. 22nd February 2023 0615 – 0920 UTC Cirrus 2

As part of a frontal system, high cirrus, with no early morning low cloud, was forecast for the ALOMAR observatory. Although the cirrus was expected to be persistent the weather front was due to bring in low cloud later in the morning. There was intermittent low cloud present at the start of the measurements however this cleared within the first few hours.

FINESSE made zenith measurements between 0615 and 0920 UTC. The INCAS aircraft overflew ALOMAR between 0820 and 0900 UTC. The aircraft sampled the cirrus at different levels by flying a racetrack pattern that ascended through the cloud between 6500 and 8000 m. This pattern was flown downwind of ALOMAR before the aircraft performed a final overpass. Figure 7 shows the trajectory of the aircraft over the observatory and the inset shows the full flight trajectory. Figure 8 shows the sky conditions above the observatory during the measurements.
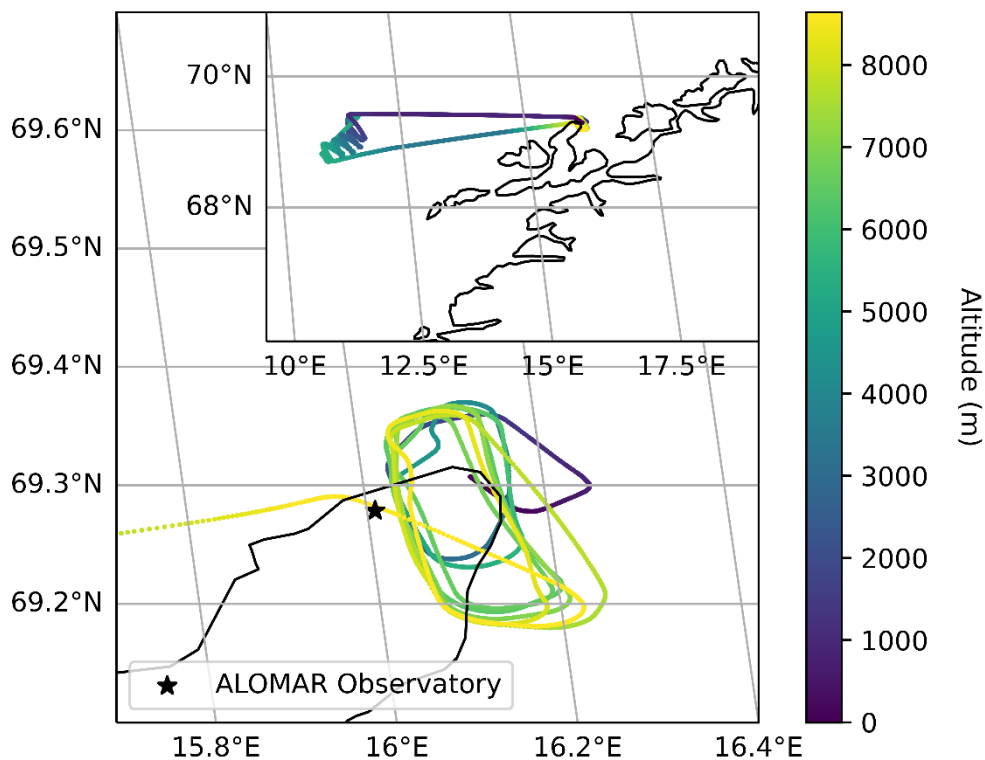

Figure 7. The trajectory of the INCAS aircraft over the ALOMAR observatory on 22nd Feb 2023. The colour represents the altitude of the aircraft. The inset plot shows the trajectory of the whole science flight.

Figure 8. The sky conditions over ALOMAR observatory on 22nd February at (a) 0622 UTC, (b) 0732 UTC, (c) 0822 UTC, the start of the INCAS aircraft overpass and (d) 0908 UTC, the end of the INCAS overpass, the contrail from the aircraft can be faintly seen in the photo. Photographs (a) and (b) from Laura Warwick, Photographs (c) and (d) from Jon Murray.

There was no 0800 UTC radiosonde due to the equipment being broken and the high humidity levels at ALOMAR did not allow the operation of the LiDAR system. The ceilometer with depolarisation installed at the ground instrumentation site began operating at 1145 UTC, having just been fixed. There was a 1111 UTC radiosonde launch from Andoya airport. The in-situ data from the INCAS aircraft and the profiles from the HATPRO offer the best opportunity to establish the vertical profile at the time of the radiance observations.

Preliminary processing of the raw data to calibrated radiances shows a clear cloud signal with small spectral variance throughout most of the time the aircraft was above ALOMAR. The radiance in the spectral window region, 800 cm^{-1} to 1200 cm^{-1}, does suggest that the cirrus was thickening with time, this was also visually observed from the surface.

3.1.4. 7th March 2023 1245 – 1530 UTC Cirrus 3

These measurements followed immediately after the Emissivity 2 measurements in section 3.2.2. The weather over Alomar was clear in the morning followed by a build-up of thin cirrus clouds from around 1245 UTC. This was forecast to be the coldest conditions in which FINESSE was run therefore a second layer of silver bubble wrap insulation was added to the instrument. The insulation around the blackbody cavities was also rearranged to leave less insulation around the cold black body. This was to enable the cold black body to cool to lower temperatures, improving the calibration.

FINESSE made zenith view measurements from 1245 UTC to 1530 UTC. The ALOMAR tropospheric LiDAR was operational from 1050 to 1740 UTC and a radiosonde was launched from Andenes airport at 1400 UTC. Measurements from the depolarising ceilometer at the ground instrumentation site were ongoing and measurements from the HATPRO started at 1053 UTC. Radiance measurements finished at 1530 UTC. Figure 9 shows the sky above the observatory at 1315 UTC.

Figure 9. The sky above the ALOMAR observatory at 1315 UTC on 7th March 2023. Photograph from Laura Warwick

3.1.5. 8th March 2023 0720 – 0925 UTC Clear sky

From 0720 to 0900 UTC FINESSE made clear sky zenith measurements. A radiosonde was released at 0800 UTC from Andoya airport. Measurements from the HATPRO and depolarizing ceilometer at the ground instrumentation site were ongoing. These measurements occurred after the snow and ice emissivity measurements discussed in section 3.2.3.

3.2. Emissivity

Surface emissivity can be retrieved from measurements of the radiance emitted by a surface, measurements of the radiation downwelling onto that surface and knowledge of the transmission between the surface and instrument (e.g., Newman et al. 2005). The emissivity of a surface is a function of angle (Li et al. 2003) and for snow surfaces the emissivity is also dependent on the density of snow and the size of the snow crystals (Huang et al. 2016). Therefore, to retrieve emissivity we made measurements of several snow samples and one ice

sample at angles of 35 and 50° from nadir and of downwelling radiation at angles of (180-35) and (180-50)° from nadir. The viewing cycle for these measurements was

1. Hot black body
2. Cold black body
3. Surface (35 or 50°)
4. Hot black body
5. Cold black body
6. Surface (35 or 50°)
7. Sky (145 or 130°)
8. Hot black body
9. Cold black body
10. Etc.

For the snow emissivity cases these measurements were accompanied by measurements of snow density and photographs of snow crystals. The snow density was measured using a metal snow density measuring tool loaned to us by Tim Carlsen from the University of Oslo. The metal snow density measuring tool was used to cut sections of a fixed volume from the snow. The tool was weighed before and after each sample was taken to determine the weight of the snow contained. The volume of the tool was specified to be 6.0 x 5.5 x 3.0 cm. Figure 10 shows the process of making a measurement of snow density.

Figure 10. The process of measuring snow density. Photographs from Laura Warwick

Snowflakes from the top layer of selected samples were then scattered onto a black felt board and photographed with a scale so that the snow grain size could be determined from the images. The scale was a knitting accessory with ruled distances and holes of various diameters. The black felt board and scale were loaned to us by Franziska Hellmuth from the University of Oslo. Figure 11 shows an example photograph of the snow crystals.

Figure 11. An example photograph showing the setup for photographing snow crystals.

3.2.1. 21st February 2023 1635 – 2150 UTC Emissivity 1

Clear conditions were forecast over ALOMAR observatory offering the opportunity to undertake snow emissivity measurements. The clear-sky conditions were forecast to be persistent from late afternoon to early morning, however intermittent low clouds in the early evening, see figure 12a, and more persistent low cloud later in the evening limited the useful observational time.

THE EUROPEAN SPACE AGENCY

Figure 12. The sky above ALOMAR on the 21st February, (a) at 1657 UTC showing low clouds (b) 1825 UTC showing clear sky. Photographs from Jon Murray.

It had snowed overnight and at the observatory there was a layer of fresher, less compact snow approximately 5 cm thick overlaying a drift of more compact older snow. The newly deposited snow was uniformly spread across the snowdrift and therefore a representative sample could be taken from most locations. Four samples of the snow were taken from the snow drift and photographs of the sampled snow crystals were taken. A flat section of snow was then carved out from the snow drift, preserving the surface as much as possible. This snow section was roughly 50 x 30 cm and around 15 cm deep. The section was placed under FINESSE so it completely filled the field of view at the angles of 35° and 50°. Figure 13 shows the setup for these measurements with the red laser spot indicating the displacement between the two angular views. FINESSE made radiative measurements of the upwelling radiance from the snow section at angles of 35° and 50° and of the downwelling radiation at angles of 145° and 130°. These measurements were made between 1635 and 2150 UTC. From 2118 UTC low clouds were seen above ALOMAR, eventually leading to the measurements being stopped. After the radiative measurements were finished, three further samples of the snow were taken and the density was measured and ice crystals photographed. Measurements from the HATPRO at the ground instrumentation site were ongoing.
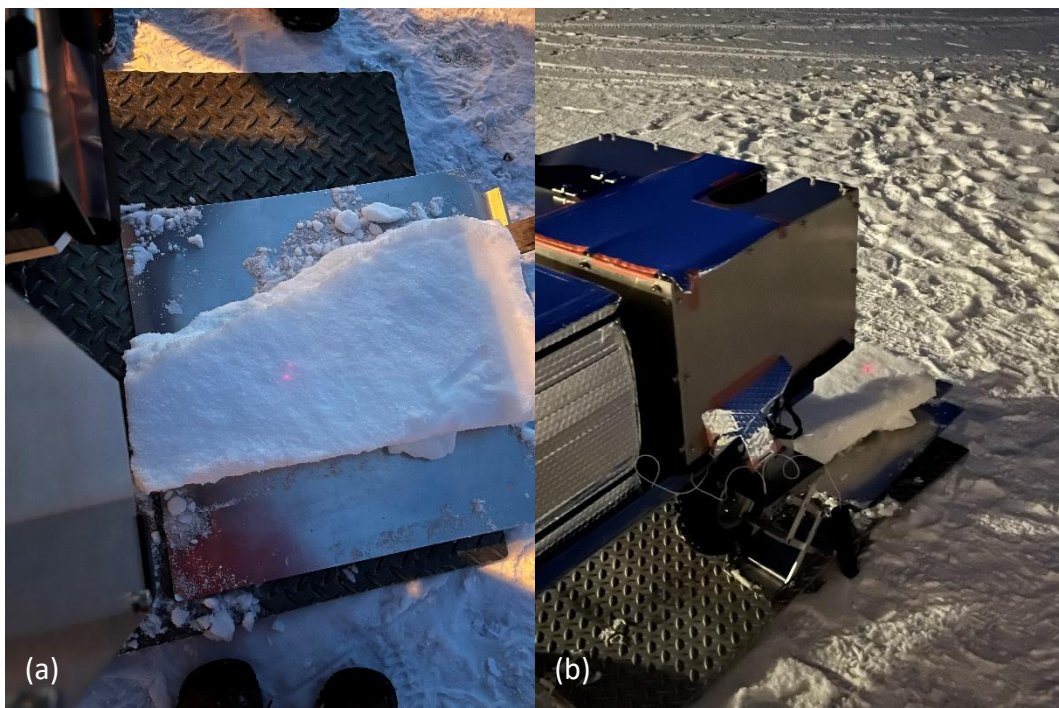

(a)   (b)

Figure 13. Photos showing the setup for the snow emissivity measurements, (a) photograph taken at 1628 UTC, the laser spot shows the view position at an angle of 35°. (b) photograph taken at 1735 UTC showing the view position for an angle of 50°. Photographs from Jon Murray.

3.2.2. 7th March 2023 1005 – 1245 UTC Emissivity 2

The weather over Alomar was clear in the morning followed by a build-up of thin cirrus clouds from around 1245 UTC. A second snow section was taken following the same procedure as on the 21st February. Four samples were taken of the snow before the radiance measurements and four further samples were taken after the radiance measurements. The density of each of these samples was measured and photographs were taken of the snow crystals. FINESSE made radiance measurements of the upwelling radiation from the surface at angles of 35° and 50° and of the downwelling radiation at angles of 145° and 130°. These measurements were made between 1005 and 1245 UTC. Figure 14 shows the setup for these measurements. A radiosonde was released from Andenes airport at 1100 UTC. The ALOMAR tropospheric LiDAR was operational from 1049 UTC. Measurements from the HATPRO started at 1053 UTC and measurements from the depolarizing ceilometer at the ground instrumentation site were ongoing. The emissivity measurements were stopped at 1245 when cirrus cloud began to impinge on the field of view, see section 3.1.4.

→ THE EUROPEAN SPACE AGENCY

Figure 14. The set up for the emissivity 2 measurements 1018 UTC. Photograph from Laura Warwick

3.2.3. 8th March 2023 0115 – 0720 UTC Emissivity 3

The weather forecast indicated clear skies would be present over ALOMAR in the early morning followed by a build-up of medium to high clouds by around 1000 UTC. A third snow section was taken using the same method as previously. Four samples of the snow were taken before and after the radiance measurements and the density of each sample was measured and the crystals were photographed. Emissivity measurements of the snow section were taken between 0115 and 0535 UTC. The ALOMAR tropospheric and RMR LiDARs were operating from 2313 to 0139 UTC. At 0250 UTC the Opus software began to hang between measurements, however at this point this only lasted a few seconds before resolving. At 0535 UTC the liquid nitrogen was topped up. At 0600 UTC the snow section was exchanged for an ice sample. Emissivity measurements of the ice sample were made between 0600 and 0720 UTC. These measurements were immediately followed by the clear sky zenith measurements in section 3.1.5. Figure 15 shows photographs of the setup for the snow and ice measurements and a photograph of the ALOMAR LiDARs.
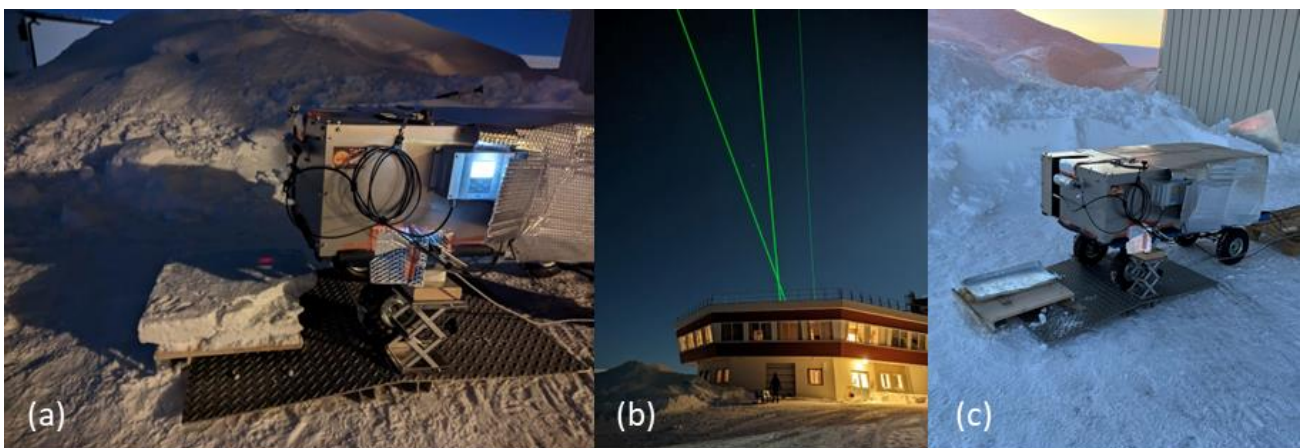

Figure 15. (a) the set up for snow emissivity measurements 0106 UTC, photograph Laura Warwick. (b) the ALOMAR LiDARs above the observatory. The fainter vertical beam is the tropospheric LiDAR mentioned in this report, photograph Laura Warwick. (c) the set up for ice emissivity measurements at 0602 UTC, photograph Jon Murray

4. SPECTRAL CALIBRATION METHOD

The interferograms recorded for FINESSE are calibrated using the measurements made of the hot and cold black body cavities during the measurement cycle. The output from the calibration procedure is the calibrated scene view radiance, $L_{scene}(\sigma)$, as a function of wavenumber, σ,

for each 1.5 s scene view interferogram. This is accompanied by the noise equivalent spectral radiance (NESR) and calibration uncertainty.

The calibration is done using a method adapted by Jon Murray from that developed by Revercomb (1988) for the High-Resolution Interferometer Sounder.

The calibrated spectral radiance is given by:

$$L_{scene}(\sigma) = e_{bb}(\sigma)L_{hbb}(\sigma, T_h) - \frac{FFT\{I(x)_{hbb} - I(x)_{scene}\}}{R(\sigma, T_h, T_c)},$$

where:

- $e_{bb}(\sigma)$ is the emissivity of the black body cavities, we assume this is 1;
- $L_{hbb}(\sigma, T_h)$ is expected radiance of the hot black body at temperature T_h calculated using the Planck function;
- T_h is the average temperature of the hot black body cavity during the hot black body views immediately before and after the measurement being calibrated;
- FFT is the fast Fourier transform;
- $I(x)_{hbb}$ is the average interferograms from the hot black body views immediately before and after the measurement being calibrated;
- $I(x)_{scene}$ is the interferogram of the scene view being calibrated and
- $R(\sigma, T_h, T_c)$ is the response function.

The response function is given by:

$$R(\sigma, T_h, T_c) = \frac{FFT\{I(x)_{hbb} - I(x)_{cbb}\}}{[e_{bb}(\sigma)L_{hbb}(\sigma, T_h) - e_{bb}(\sigma)L_{cbb}(\sigma, T_c)]},$$

where cbb refers to the cold black body and all other symbols have the same meaning. Figure 17 shows an example of the instrument response function. Further details and justification of this procedure can be found in section 5.1.2 of Warwick (2023).

The NESR is calculated by differencing consecutive individual calibrated zenith scans. This is only done when there is no significant variation in the spectral information. The NESR was found to be consistent across all six measurement days. The calibration error was calculated for each individual 1.5 second spectrum. It was found by calculating the maximum change in

calibrated radiance caused by a change of 1 K in the temperature of the hot black body and 0.25 K in the temperature of the cold black body.
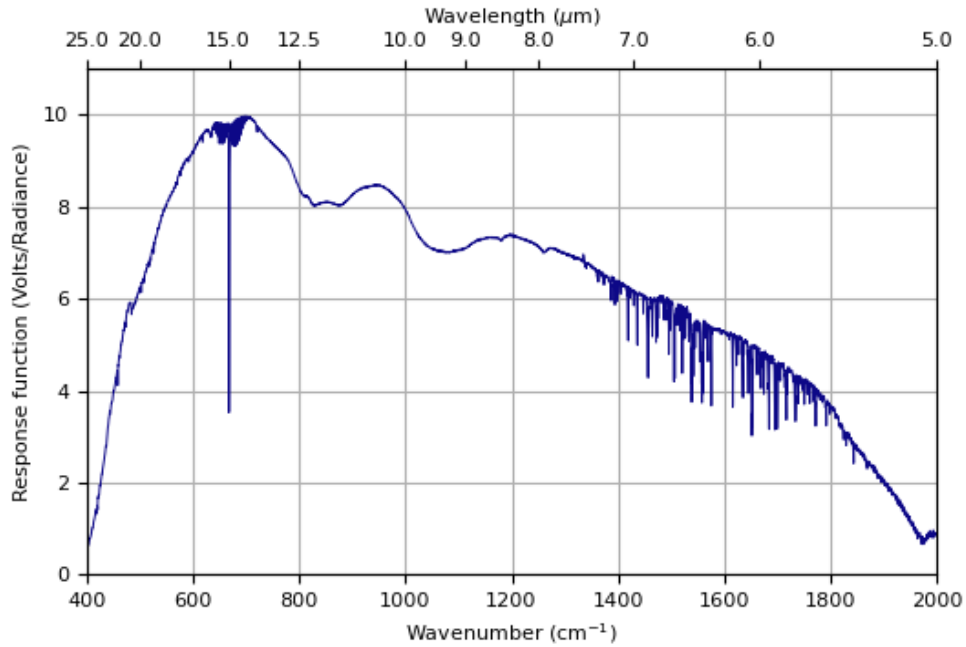

Figure 17. The FINESSE instrument response function at ~0800 UTC on 8th Feb 2023

→ THE EUROPEAN SPACE AGENCY
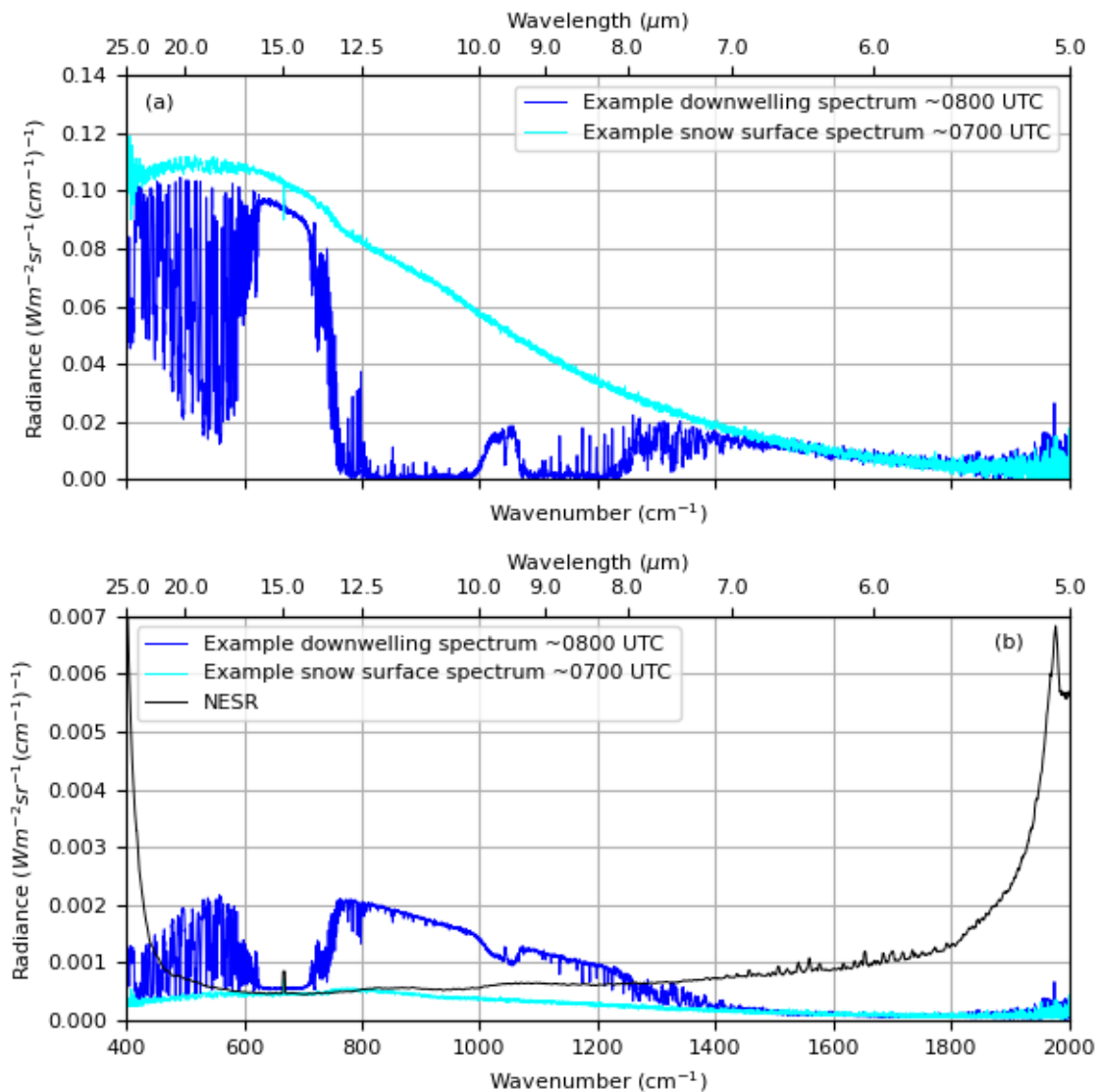
Figure 18. (a) Example downwelling and snow spectra taken on 8th March 2023. Each spectrum is a single 1.5 s acquisition. (b) Calibration error for the downwelling and snow surface spectra and the NESR.

5. EXAMPLE CALIBRATED SPECTRA

Figure 19 shows a selection of calibrated spectra for different cases and measurement days. The low radiance seen in the far infrared micro-windows between 400 and 500 cm^{-1} in the clear sky case (figure 19a) shows that the atmosphere is very dry. The effect of the cirrus cloud thickness can be seen when comparing the spectra in figures 19b and 19c. This difference is present across the atmospheric window between 750 and 1250 cm^{-1} and in the far-infrared micro-windows. This suggests that information about the cirrus cloud properties can be inferred

from the far-infrared. The final spectrum (figure 19d) is an example upwelling spectrum from a snow surface.
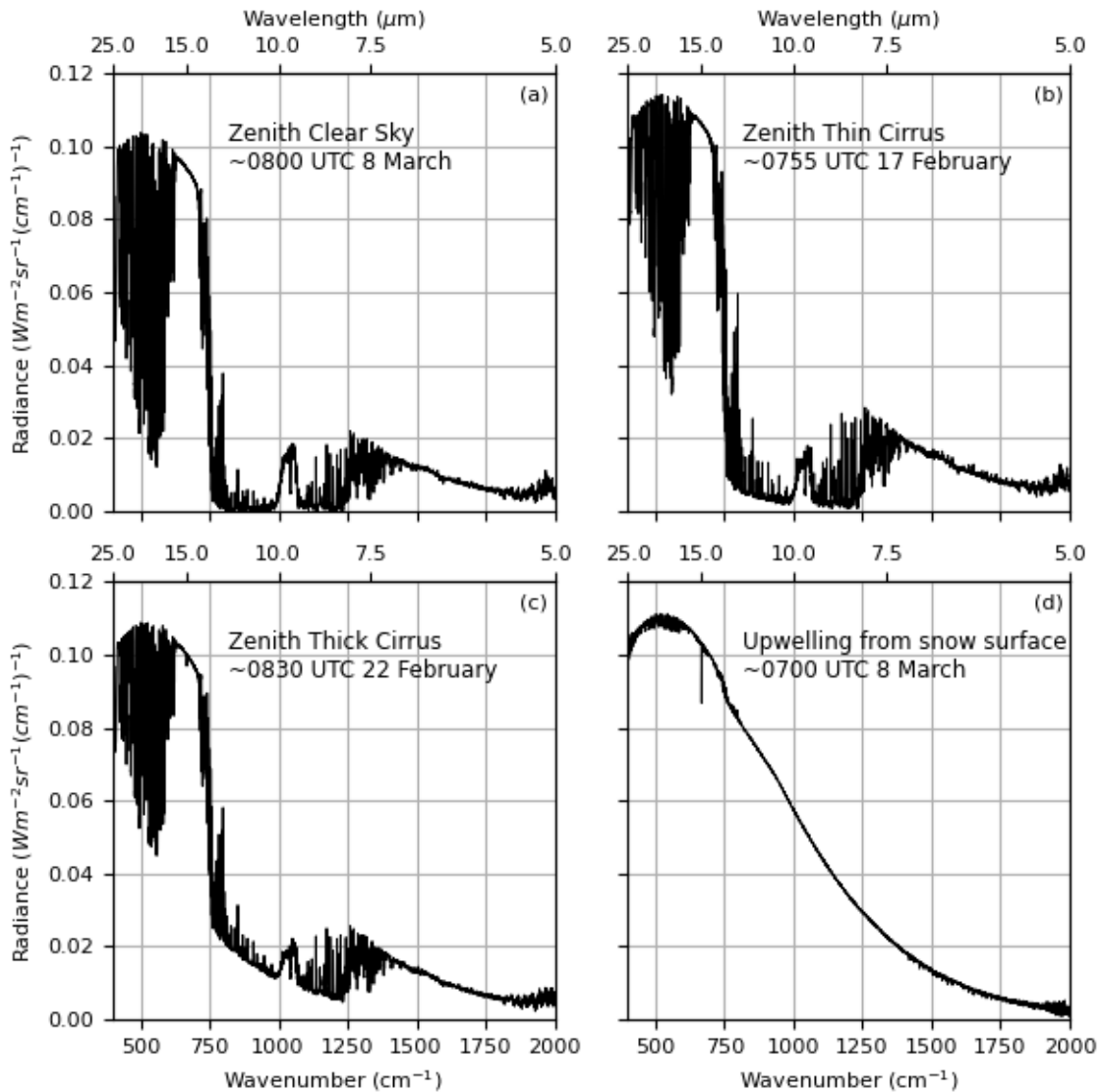
Figure 19. Example calibrated spectra from the campaign. (a) A clear sky view from 8th March, (b) a thin cirrus cloud from 17th February, see figure 5, (c) a thick cirrus cloud from 22nd February, see figure 8, (d) the upwelling radiance signal from a snow surface from 8th March, see figure 15. Each plotted spectrum covers a period of 1 minute and is the average of 40 individual spectra.

6. INSTRUMENT PERFORMANCE

A first test of the instrument performance is to plot the change in the response function over time. Figure 20 shows the percentage difference between the response function for an individual measurement cycle and the average response function calculated over the whole measurement time that day. This is plotted for 4 wavenumbers. We use the stability of the

instrument response function over time as a way of determining the stability of the instrument. The large changes in the response function that can be seen on the 21st of Feb and 8th of March were caused by topping up FINESSE's liquid nitrogen dewar during the measurements.

Across all six days, the change in the response function exhibits a long-term drift over the timescale of several hours. This is likely due to the changing external conditions experienced by FINESSE. This long-term drift does not affect the quality of the calibrated radiances due to the frequency of the FINESSE calibration views. There is also a shorter-term variation in the response function on the timescale of several minutes. This scatter is larger for lower wavenumbers being approximately ±1.5% at 410 cm^{-1} and less than ±0.5% at 900 cm^{-1}. The larger scatter is expected at the lower wavenumbers as the response function is lower at 410 cm^{-1} as this is nearing the limit of FINESSE's sensitivity. This short-term variation in the response function is smaller than the uncertainty in the response function caused by uncertainty in the temperatures of the black body cavities.
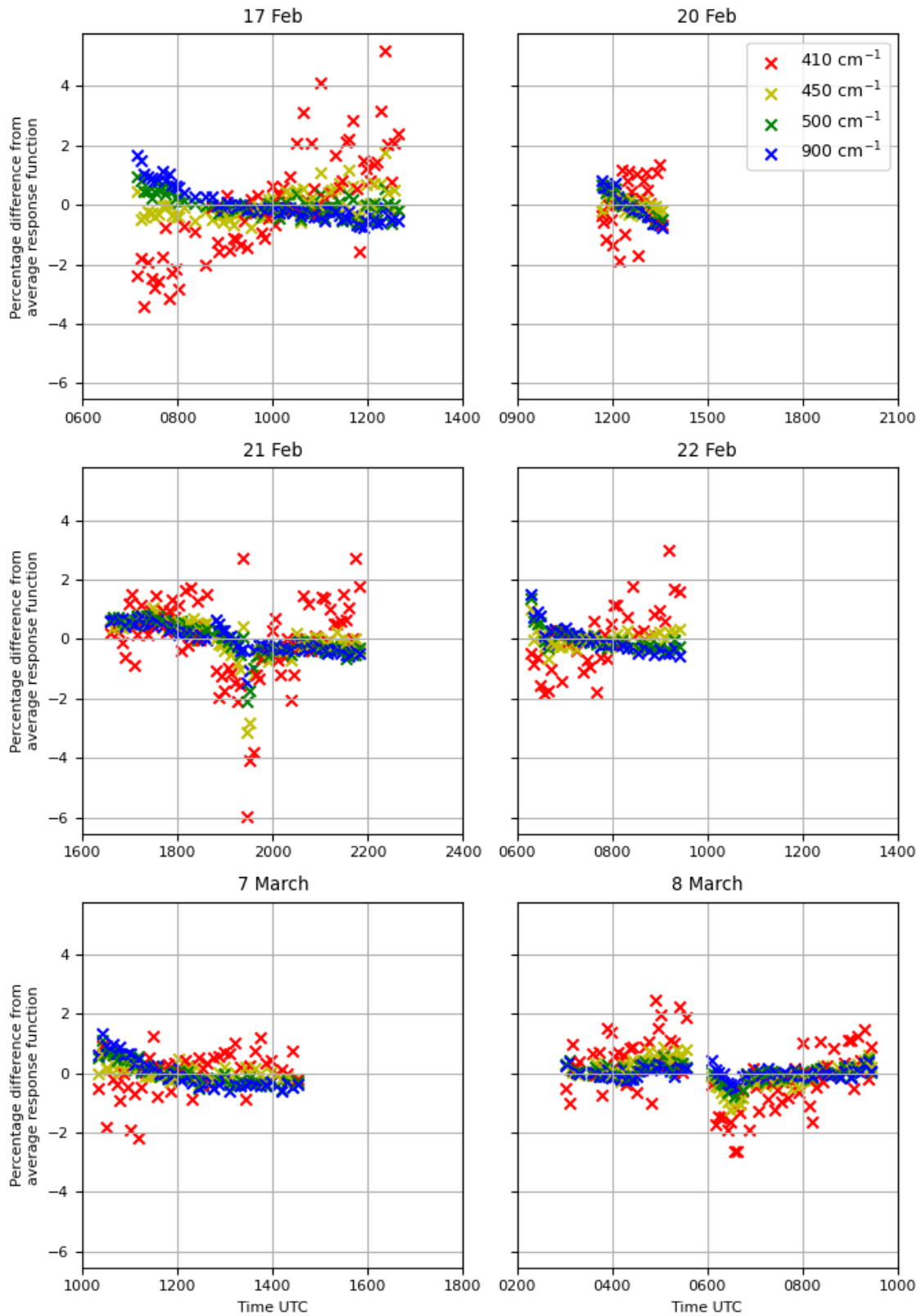
Figure 20. The percentage change in the response function against time for the 6 days of measurement. The x-scale covers the same time range in each case.

→ THE EUROPEAN SPACE AGENCY

7. CONCLUSIONS AND RECOMMENDATIONS FOR USE OF DATA

Overall, the campaign successfully met its aims. The key outcomes are summarised below along with suggestions for the use of the data.

1. FINESSE was deployed in an Arctic environment for the first time.
2. The FINESSE response function was shown to have good stability and the instrument functioned successfully in the cold and windy conditions.
3. Two contrasting cirrus cloud cases were measured by FINESSE with co-incident in-situ measurements of ice cloud properties from aircraft. This data could be used in forward modelling studies to test the performance of different ice cloud models. Alternatively, the data could be used to perform retrievals of ice cloud properties which can then be validated against in-situ measurements. This is important for the validation of ice cloud models in the far-infrared, particularly as these models will be required for FORUM.
4. Measurements were made of three snow surfaces and one ice surface for the purpose of retrieving surface emissivity. These emissivity retrievals will help to improve the limited knowledge of surface emissivity in the far infrared and are important for the validation of FORUM emissivity retrievals.
5. The downwelling radiance was also measured in clear sky conditions and under changeable conditions with scattered low cloud. These data could be used for intercomparison between other instruments deployed on the field campaign. Temperature and water vapour retrievals could also be performed using the clear sky data.

8. EXPLAINATION OF DATA FORMAT

The spectra recorded by FINESSE are provided in netCDF files. Each netCDF file contains either zenith or emissivity measurements for the period indicated in the title. The netCDF files also contain auxiliary data including the NESR, calibration error, response functions and hot black body temperatures used for calibration. The NESR is the same for every spectrum however the calibration error varies per spectrum.

The spectra are grouped by cycle. Each cycle consists of several target views interspersed with calibration views. The calibration views are not recorded in the netCDF file. The number of target views per cycle varies between netCDF files. Each target view consists of 40 individual spectra each with an acquisition time of 1.5 seconds. This means that each target view lasts approximately 1 minute.

The attributes of an example netCDF file are shown below:

NetCDF Global Attributes:

title: 'Calibrated radiances from FINESSE for Alomar measurements taken on the 8th March 2023'

instrument: 'FINESSE'

institution: 'Imperial College London'

author: 'J.E.Murray, Imperial College London.'

contact: 'j.murray@imperial.ac.uk'

measurement_date: '2023-Mar-8'

hbb_error: '1.00K' *uncertainty in the temperature of the hot black body used to calculate the calibration error*

cbb_error: '0.25K' *uncertainty in the temperature of the cold black body used to calculate the calibration error*

history: '

[2023-04-17] Produced by Jon Murray in .sav format

[2023-04-26] Reformatted to netCDF by Laura Warwick

[2023-04-26] Calibration error calculated by Laura Warwick

[2023-05-12] wn stretch of 1.000160 applied and data resampled'

version: '1_1'

comment: '

These observations were made to derive surface emissivity snow scattered on an ice surface at the two angles of 35 and 50 degrees.

The BRUKER GUI used an automated script file to cycle between calibration (hot/cold), surface (35/50) and sky (145/130) views. For these measurements there were 5 measurement cycles. Each measurement cycle consists of 2 scene views and 1 views of each calibration target in the order:

1 hot bb

1 cold bb

1 surface view, this was alternated between 35 and 50 degrees from nadir
1 sky view, this is (180-surface view angle)

For each view the EM27 records 40 interferograms. The scan time for each
interferogram is approximately 1.5 s. Each view is therefore roughly 1
minute of observations and each measurement cycle lasts approximately 7
minutes.'

NetCDF dimension information:

> **Name: cycle_index**   *number of measurement cycles in file*
>> size: 5
>
> **Name: view_index**   *number of target views per measurement cycle*
>> size: 2
>
> **Name: int_index**
>> size: 40   *number of interferograms per target view*
>
> **Name: bb_index**
>> size: 2   *The spectra are calibrated using the average of*

the hot black body temperatures before and after the target view

> **Name: wavenumber**
>> size: 8500

NetCDF variable information:

> **Name: wn**
>> dimensions: ('wavenumber',)
>>
>> type: dtype('float64')
>>
>> units: 'cm-1'
>>
>> long_name: 'Wavenumber'
>
> **Name: rad**
>> dimensions: ('cycle_index', 'view_index', 'int_index',
'wavenumber')
>>
>> type: dtype('float64')
>>
>> units: 'W / (m2 sr cm-1)'
>>
>> long_name: 'Radiance'
>
> **Name: nesr**
>> dimensions: ('wavenumber',)
>>
>> type: dtype('float64')

```
                    units: 'W / (m2 sr cm-1)'
                    long_name: 'Noise Equivalent Spectral Radiance'
        Name: angle
                    dimensions: ('cycle_index', 'view_index', 'int_index')
                    type: dtype('float64')
                    units: 'degrees from nadir'
                    long_name: 'Mirror Angle'
        Name: time
                    dimensions: ('cycle_index', 'view_index', 'int_index')
                    type: dtype('float64')
                    units: 'seconds since midnight'
                    long_name: 'Scan time'
        Name: resp
                    dimensions: ('cycle_index', 'wavenumber')
                    type: dtype('float64')
                    units: 'Volts per (W / (m2 sr cm-1))'
                    long_name: 'Response Function'
        Name: resp_time
                    dimensions: ('cycle_index',)
                    type: dtype('float64')
                    units: 'Seconds since midnight'
                    long_name: 'Time of Response Function'
                    comment: 'Time for the response functions in the resp
variable'
        Name: hbb_temp
                    dimensions: ('cycle_index', 'bb_index')
                    type: dtype('float64')
                    units: 'degK'
                    long_name: 'Hot Blackbody Temperature'
                    comment: 'The average of bb_index 0 and 1 are used to
calibrate the spectrum'
        Name: cbb_temp
                    dimensions: ('cycle_index', 'bb_index')
                    type: dtype('float64')
                    units: 'degK'
```

```
                    long_name: 'Cold Blackbody Temperature'
                    comment: 'The average of bb_index 0 and 1 are used to
calibrate the spectrum'
          Name: lower_cal_error
                    dimensions: ('cycle_index', 'view_index', 'int_index',
'wavenumber')
                    type: dtype('float64')
                    units: 'W / (m2 sr cm-1)'
                    long_name: 'Lower Calibration Uncertainty'
                    comment: 'Lower calibration uncertainty caused by
uncertainty in the HBB temperature of +/-1.00K and in the CBB temperature
of +/-0.25K'
          Name: upper_cal_error
                    dimensions: ('cycle_index', 'view_index', 'int_index',
'wavenumber')
                    type: dtype('float64')
                    units: 'W / (m2 sr cm-1)'
                    long_name: 'Upper Calibration Uncertainty'
                    comment: 'Upper calibration uncertainty caused by
uncertainty in the HBB temperature of +/-1.00K and in the CBB temperature
of +/-0.25K'
```

Data logs from the Vaisala PTU300 pressure, temperature, humidity sensor and the Vaisala GMP343 CO_2 sensor are also provided as ASCII files.

The pressure, temperature, humidity files contain 4 tab-separated columns:

1. Date and time (UTC)
2. Pressure (hPa)
3. Temperature (°C)
4. Humidity (%)

The CO_2 files contain 3 tab-separated columns:

1. Date and time (UTC)
2. CO_2 concentration (ppm)
3. Temperature inside the sensor (°C)

9. REFERENCES

Calcan, A.; Stefan, S.; Vajaiac, S.N. and Moaca, D. (2020) Airborne measurements in different clouds. INCAS Bulletin 13(1) 19-28. https://doi.org/10.13111/2066-8201.2021.13.1.3

Li Z.-L.; Wu, H.; Wang, N.; Qiu, S.; Sobrino, J.A.; Wan, Z., Tang, B.-H. and Yan, G. (2013) Land surface emissivity retrieval from satellite data, International Journal of Remote Sensing, 34(9-10) 3084-3127, https://doi.org/10.1080/01431161.2012.716540

Newman, S.M.; Smith, J.A.; Glew, M.D.; Rogers, S.M. and Taylor, J.P. (2005), Temperature and salinity dependence of sea surface emissivity in the thermal infrared. Q.J.R. Meteorol. Soc., 131 2539-2557. https://doi.org/10.1256/qj.04.150

Revercomb, H.E.; Buijs, H.; Howell, H.B.; LaPorte, D.D.; Smith, W.L. and Sromovsky, L.A. (1988) Radiometric calibration of IR Fourier transform spectrometers: solution to a problem with the High-Resolution Interferometer Sounder, Appl. Opt. 27, 3210-3218, https://doi.org/10.1364/AO.27.003210

RPG-Radiometer Physics (2013) Technical Instrument Manual: RPG-MWR-STD-TM. Available from: https://www.radiometer-physics.de/downloadftp/pub/PDF/Radiometers/General_documents/Manuals/2015/RPG_MWR_STD_Technical_Manual_2015.pdf Accessed 25-April-2023.

Schäfer, B; Carlsen, T; Hanssen, I; Gausa, M and Storelvmo, T. (2022) Observations of cold-cloud properties in the Norwegian Arctic using ground-based and spaceborne lidar. Atmos.Chem. Phys 22 9537-9551. https://doi.org/10.5194/acp-22-9537-2022

SPEC (2012) Hawkeye Combination Cloud Particle Probe. Available from: http://www.specinc.com/hawkeye-combination-cloud-particle_probe Accessed 24-May-2023

Vaisala (2022) Lidar Ceilometer CL61 Datasheet B211780EN-G. Available from: https://docs.vaisala.com/v/u/B211780EN-G/en-US Accessed 25-April-2023.

→ THE EUROPEAN SPACE AGENCY

Warwick, L (2023) Measuring tropospheric water vapour and surface emissivity using far-infrared radiances. PhD Thesis. Imperial College London.

→ THE EUROPEAN SPACE AGENCY